Soil Stabilization Properties of Flexible Intruders

by

Katharine Luginbuhl

Submitted to the
Department of Mechanical Engineering
in Partial Fulfillment of the Requirements for the Degree of

Bachelor of Science in Mechanical Engineering

at the

Massachusetts Institute of Technology

June 2012

Signature of Author .....
Department of Mechanical Engineering
May 10, 2012

Certified by .....
Anette E. Hosoi
MacVicar Faculty Fellow, Associate Professor of Mechanical Engineering
Thesis Supervisor

Accepted by .....
John H. Lienhard V
Samuel C. Collins Professor of Mechanical Engineering
Undergraduate Officer

Soil Stabilization Properties of Flexible Intruders

by

Katharine Luginbuhl

Submitted to the Department of Mechanical Engineering
on May 10, 2012 in Partial Fulfillment of the
Requirements for the Degree of

Bachelor of Science in Mechanical Engineering

ABSTRACT

In many locations, soil is held in place by the roots of plants. When these plants are removed or die, the soil loses its cohesive strength and erodes away. We seek to create artificial soil stabilizers that use the same physical principles as the plant roots. To investigate how flexible materials can stabilize soil, we use photoelastic particles to analyze the forces within a system when a flexible intruder is introduced to the system. We report on the increase in system forces as an effect of the flexible intruder and compare it to experiments with plant roots. Since soil is a granular material, using this method to increase the forces within patches of soil may help prevent erosion or landslides.

Thesis Supervisor: Anette E. Hosoi

Title: P MacVicar Faculty Fellow, Associate Professor of Mechanical Engineering

ACKNOWLEDGMENTS

Thanks to: Dawn Wendell, for being the best grad student a UROP could hope for, and Professor Hosoi, for being so inspirational and helpful that it's probably a superpower.

TABLE OF CONTENTS

LIST OF FIGURES

LIST OF TABLES

1. INTRODUCTION

The phenomenon of soil stabilization by use of plant roots is well documented. This is especially true for soil on steep slopes. The forces various types of roots can exert on soils, as well as the strength of the roots themselves, have been extensively studied [1]. These studies have been done in an attempt to determine the optimal plant type to use when creating artificial slopes.

Previous studies have also compared the efficiencies of roots digging through soil and of flexible intruders digging through soil [2]. The forces exerted by the roots on the soil were considered as well. As well as energy-efficient digging, the stabilization properties of flexible intruders hold interest. Because flexible intruders in soil behave in a way comparable to roots, they could potentially be used in soil stabilization in the future. These flexible intruders could supplement or replace roots in helping to prevent soil erosion.

2. BACKGROUND

2-1. Photoelasticity

Certain materials exhibit birefringence, meaning light passing through them splits into two distinct beams. When this happens, the polarity of the light can also be altered. In order to detect only light which has been altered in this manner, two oppositely-handed circular wave polarizers are used. Because all light would normally be blocked by two oppositely-handed polarizers, placing a birefringent material between two oppositely-handed polarizers will allow only light with an altered polarity through both filters.

Materials which exhibit photoelastic behavior become birefringent when stressed. This photoelastic behavior causes a distinct pattern of birefringence for a given stress. As the stress increases, the number of fringes caused by the birefringence also increases. This stress can be calibrated, and is being directly proportional to the sum of the square of the changes in intensity over a particle. A computer analysis method of determining the forces in a system from a photographic image of the system using this method is described in Appendix A. Because the particles used in this experiment are round, all contacts are treated as points, to allow easier comparison of the stresses between particles.

2-2. Roots

One of the main motivations to study the effect of flexible intruders on a granular system is based on the effects roots have in soil and sand. The technique of a system of photoelastic particles has previously been used to study the effect of roots growing through a granular system, in order to attempt to mimic the energy-efficient path finding of roots with a mechanical digger [2]. An image of the roots growing between the photoelastic particles is shown in Figure 2-1. Figure 2-2 shows the same system after the root grew through it. Note that the particles were stressed by the growth of the roots in the system.

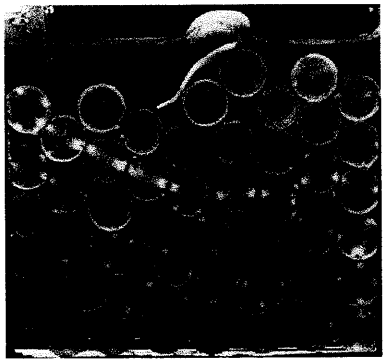

Figure 2-1: A system of photoelastic particles at the start of a root growth experiment.

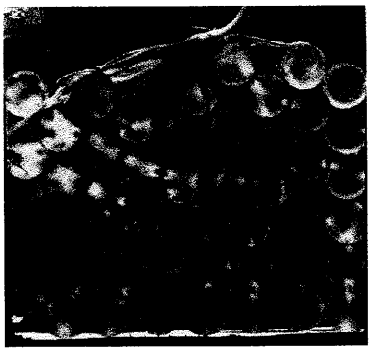

Figure 2-2: A system of photoelastic particles being stressed by the roots of a pinto bean plant.

This method showed that roots would grow through certain forces and around others. These experiments also showed that the threshold force increased with the age of the root. These previous experiments were additionally used to determine the change in force between particles after the roots had grown. The probability density of the forces exerted by the roots on the particles is given in Figure 2-3.

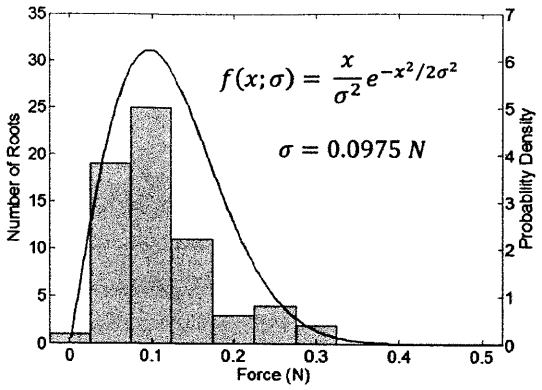

Figure 2-3: The probability density of the force exerted by a pinto bean root.

3. METHODS

3-1. Apparatus

The system used to measure forces consisted of 47 cylindrical photoelastic particles made of polyurethane, each with a diameter of 9.13 ±0.16mm and a height of 6.31 ±0.09mm. The particles were cut in the Schlumberger labs, using a waterjet. These particles were placed in a box made of acrylic with a height of 75.2 mm, a width of 76.1mm, and a depth of 6.9mm, which was just large enough for the particles to fit in the box without a significant amount of frictional forces. On each side of the acrylic box, oppositely-handed circular wave polarizers were attached in such a manner as to block all light except for the light changed in polarity by the birefringence of the photoelastic particles. In this manner, the birefringence caused by the photoelastic particles under force could be directly observed. This system is shown in Figure 3-1.

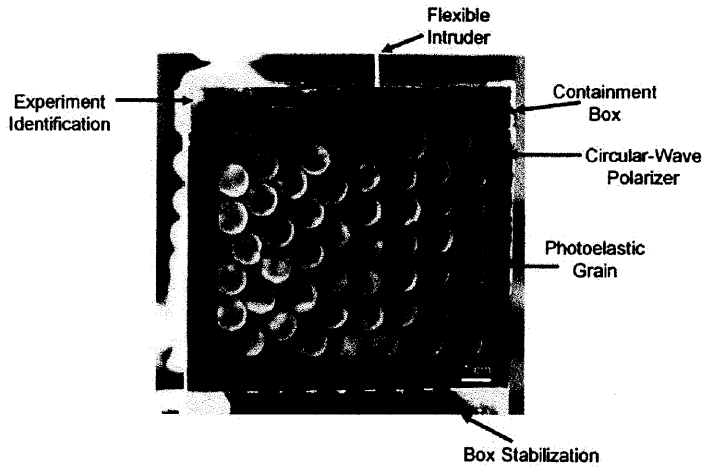

Figure 3-1: The experimental system used.

In order to apply a prescribed force to the system, a texture analyzer was used. A variety of 6 mm wide strips of flexible plastic and aluminum with various thicknesses were attached to the texture analyzer. These strips were attached such that they would deflect in the plane of the particle system. Strips of 128 mm long polycarbonate with a stiffness of 2 GPa were used, as well as strips of 153.5 mm long aluminum with a stiffness of 70 GPa. A Canon PowerShot SD700IS camera was used to record the image of the photoelastic particles before and after the force had been applied to the system. Figure 3-2 shows a sample photograph of a box of particles before the experiment, and Figure 3-3 shows a box of particles while under 1 newton of force from 0.635 mm-thick polycarbonate.

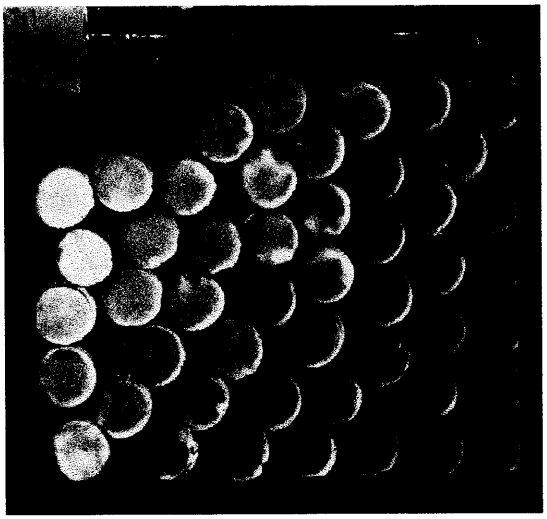

Figure 3-2: A box of particles before the experimental force had been applied.

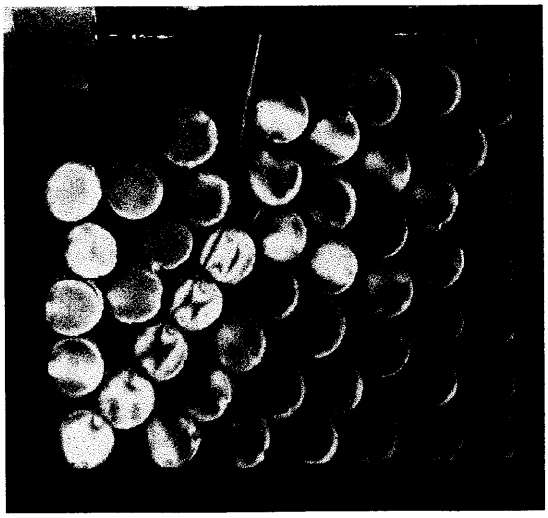

Figure 3-3: The box of photoelastic particles after 1 newton of force had been applied by 0.635 mm-thick polycarbonate.

3-2. Procedure

For each experiment, a picture was taken of the acrylic box and photoelastic particles before any forces were applied. The texture analyzer was then used to lower the top of the flexible intruder at 1 mm/s until a force of 1 newton was reached, at which time it stop until the reset button was pressed. While the texture analyzer was stopped, a picture was taken of the new, stressed system. After the picture was taken, the reset button was pressed, and the texture analyzer would raise the top of the flexible intruder at 1 mm/s until it returned to its original point. Data was collected from the time the texture analyzer encountered more than .01 newton of force until the texture analyzer returned to the point where it had first encountered that force. Figure 3-4 shows a sample force versus displacement graph from the texture analyzer where the flexible intruder did not buckle. If the flexible intruder buckled, and the texture analyzer was unable to reach the maximum force, the photograph was taken at the same time the reset button was pressed, shortly before the flexible intruder started to plastically deform.

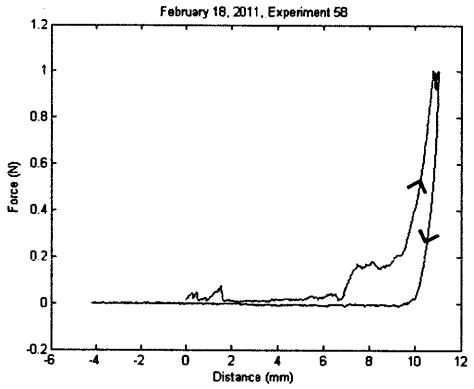

Figure 3-4: A sample force versus displacement graph from the texture analyzer during an experiment where the flexible intruder did not buckle.

Experiments were done in pairs, with the flexible intruder changed between each pair of experiments. Between each experiment, the photoelastic particles were jumbled so as to randomize the packing arrangement. Between each pair of experiments, the particles were removed from the box and then replaced, so as to further increase the randomness of the particle arrangement.

4. DATA

In order to collect the data for the experiment, both the data from the texture analyzer and the photographs of the photoelastic particles were used. In order to determine the forces acting within the particle system, a series of photographs of the photoelastic particles under known forces were used, and the patterns of light from the photoelastic particles matched manually. Figure 4-1 shows a sample photograph of a particle under a 1 newton of force. The forces were then totaled for each photograph from the system.

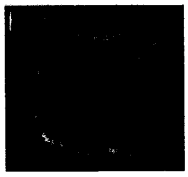

Figure 4-1: The light patterns on a photoelastic particle under 1 newton of force.

Unfortunately, the intensity squared method for automatically determining the total forces in a system could not be used. There are several causes for this problem. The first is the particles themselves, which were not completely regular. While the diameters of the particles was roughly constant to within about 2%, the edges of the particles were rough rather than smooth, due to process for cutting them on the waterjet. Both the polarizers and the acrylic boxes used, rather than being perfectly uniform, had a number of scratches on them. Finally, the camera used was low enough quality that at high forces, the bands in the particles blurred on the captured image. These factors combined to make the automatic computation of the forces in the system much less accurate than manually comparing them to a series of calibration photographs. The resulting intensity squared from the program as a function of applied force is shown in Figure 4-2, which clearly demonstrates the imprecision in such a computation method by providing multiple data points at a given force.

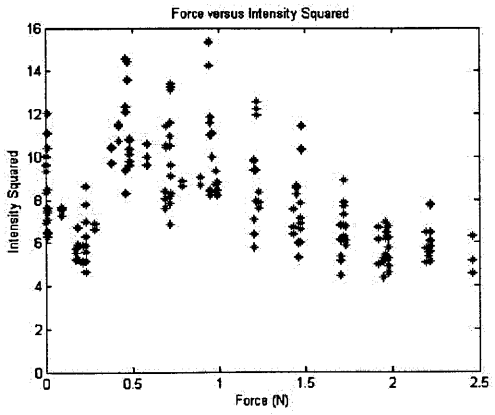

Figure 4-2: The computed intensity squared as a function of applied force on a single particle. Note the high imprecision.

Once the forces on each particle were determined, it was desirous to be able to compare the forces exerted by the flexible intruders to the forces exerted by the plant roots. As seen in Figure 2-3, the plant roots exert a mean force of 0.098 N. Figure 4-3 shows the distribution of the forces exerted on the particles by the flexible intruders. The flexible intruders exert a mean force of about 0.26 N, or roughly three times the force exerted by the plant roots.

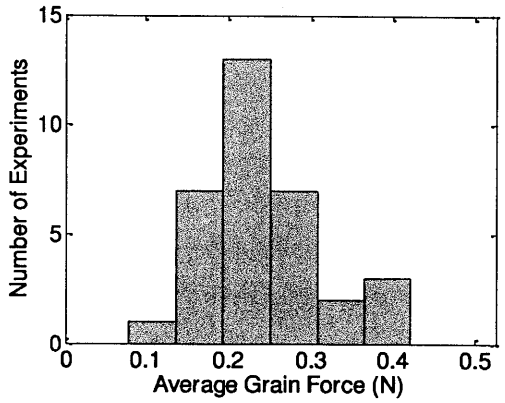

Figure 4-3: The distribution of the forces on individual grains from the flexible intruders.

Because of the complexity of the system, both the summed total forces in each system and the number of particles under force were computed. As the system had a constant number of particles in each experiment, the average force on all the particles would simply be a multiple of the total force, so an averaged force was gained from the total system forces divided by the number of particles under force. Figure 4-4 shows the total forces in the system, and figure 4-5 shows the number of particles under force, both as a function of intruder thickness and material.

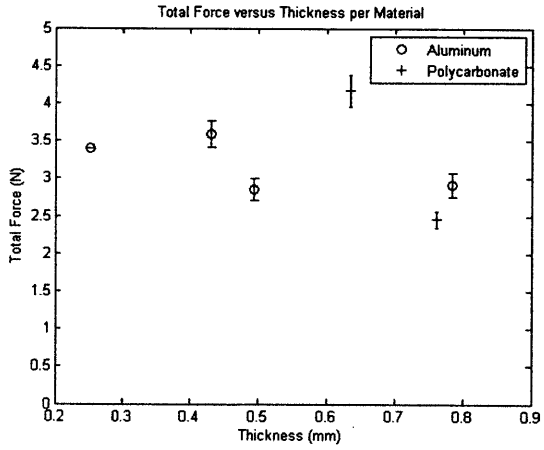

Figure 4-4: The total summed forces in the system as a function of intruder thickness and material.

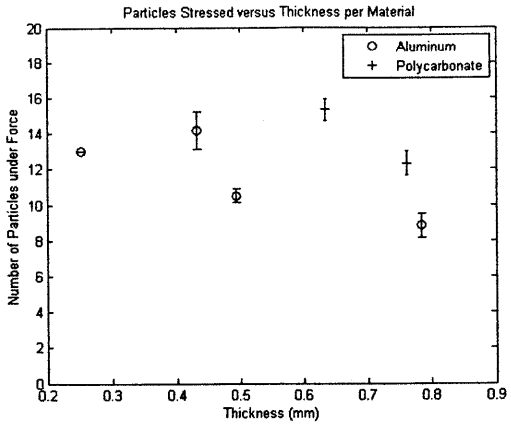

Figure 4-5: The average number of particles under force in the system as a function of intruder thickness and material.

To analyze the data from the texture analyzer, the displacements at the top of the flexible intruder, as well as the forces applied at those displacements, were used. The displacements and forces were recorded every 5 μm. By multiplying the changes in displacement by the average force applied at the two displacements in question, and computing the sum over the entire downward displacement, the total work done to the system could be computed.

In order to properly compare the aluminum and polycarbonate flexible intruders, the effective stiffness of the flexible intruders was computed as a function of Young's modulus, the area moment of inertia for the intruder, and the length of the intruder. The EI of each intruder was then computed using the effective stiffness and the moment. These results are summarized in table 4-1.

TABLE 4-1: Physical properties of the various flexible intruders used.

material	thickness (mm)	length (mm)	width (mm)	young's modulus (GPa)	I (m^4)	effective stiffness (N/m)	EI ($N*m^3$)
aluminum	0.252	153.5	6.0	70	$8.002*10^{-15}$	0.0238	$1.902*10^{-16}$
aluminum	0.432	153.5	6.0	70	$4.031*10^{-14}$	0.1198	$4.828*10^{-15}$
aluminum	0.495	153.5	6.0	70	$6.064*10^{-14}$	0.1802	$1.093*10^{-14}$
aluminum	0.785	153.5	6.0	70	$2.419*10^{-13}$	0.7186	$1.738*10^{-13}$
polycarbonate	0.635	128	6.0	2	$1.280*10^{-13}$	0.0156	$2.001*10^{-15}$
polycarbonate	0.762	128	6.0	2	$2.212*10^{-13}$	0.0270	$5.974*10^{-15}$

Because of the highly stochastic nature of the system, multiple tests were run for each thickness of each material. The average values of summed forces, number of particles, work into the system, and maximum intruder displacement were then computed. These results are shown in Table 4-2.

TABLE 4-2: Averaged values for summed forces in the system, number of particles under force, work into the system, and maximum intruder displacement as a function of intruder effective stiffness.

EI ($N*m^3$)	summed forces (mN)	number of particles under force	work into the system (mJ)	maximum intruder displacement (mm)
$1.902*10^{-16}$	340.0	13.0	1.30	57.7
$4.828*10^{-15}$	359.2 ± 17.3	14.2 ± 1.1	4.54 ± 0.36	28.0 ± 1.8
$1.093*10^{-14}$	286.3 ± 14.5	10.5 ± 0.4	3.57 ± 0.23	27.4 ± 1.6
$1.738*10^{-13}$	291.7 ± 16.7	8.8 ± 0.7	4.04 ± 0.39	27.4 ± 2.2
$2.001*10^{-15}$	416.6 ± 21.5	15.3 ± 0.6	8.60 ± 0.55	36.3 ± 1.5
$5.974*10^{-15}$	254.8 ± 11.3	12.3 ± 0.4	8.26 ± 0.71	23.5 ± 1.9

The data presented here corresponds only to experiments during which the flexible intruder did not buckle. Because of this, there is only one set of data available for the aluminum intruder with thickness 0.252 mm, or EI $1.9021*10^{-16}$ $N*m^3$. This lack of additional data is also why that set of data has no standard error bounds in Table 4-2.

5. RESULTS

One important component for stability is the length of the force chains in the granular medium. Longer force chains are more desirous, as they contain more soil. This means that for a given number of force chains, more soil will be held in place. Longer force chains allow soil further from the generated source to be contained, enabling the use of fewer force inputs for the same area of soil. Figure 5-1 shows the number of particles under force, and thus the approximate length of the force chain generated, as a function of the EI of each flexible intruder. From this graph, a trend of longer force chains in more flexible intruders can be seen.

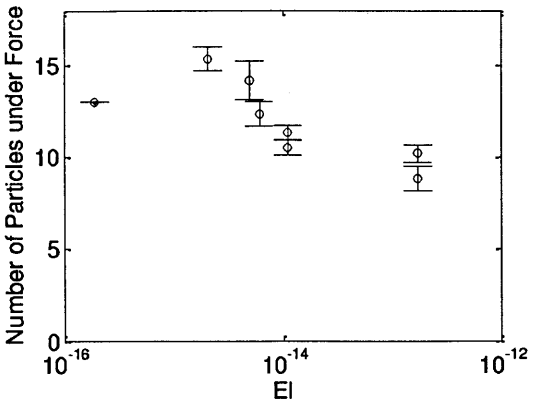

Figure 5-1: Number of particles under force as a function of the EI of each flexible intruder.

Another important component is the strength of the force chains. A stronger force chain will be able to withstand more external forces. Figure 5-2 shows the strength of the force chains as a function of the EI of each flexible intruder.

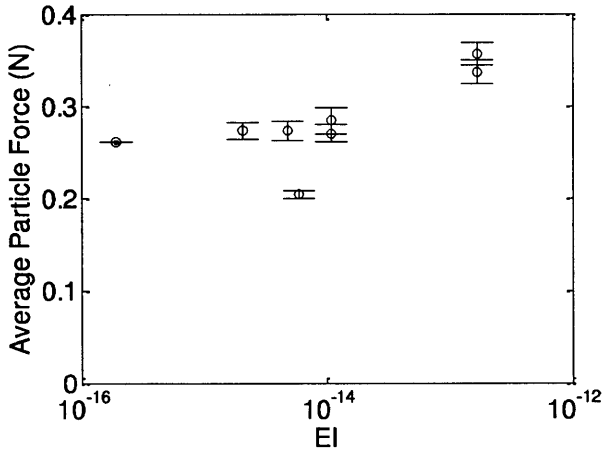

Figure 5-2: The average force on the stressed particles as a function of the EI of the flexible intruders.

Additionally, in order to compute the efficiency of each intruder, a method of determining the increase in energy of the system was needed. The multiplication of the summed total forces in the system by the maximum intruder displacement was chosen to provide the appropriate units of energy while still encompassing important parameters. Figure 5-3 shows the efficiency of the intruder as a function of its EI. This result matches the result from experiments of flexible intruders in a fine granular medium in which the overall depth of the intruders was measured [2].

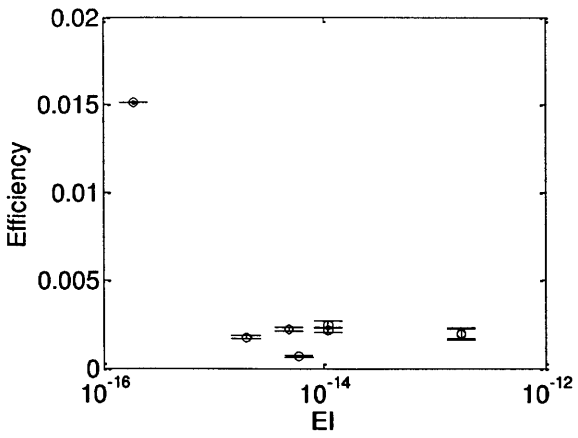

Figure 5-3: Energy efficiency of each intruder as a function of effective stiffness. Energy efficiency is computed by comparing the input energy from the texture analyzer with the energy in the forced system.

Future experiments with more data would provide more conclusive results. Here, only two materials were tested, and owing to the large amount of buckling in the thinner flexible intruders, only eight discreet data points were generated, one of which lacks appropriate error bars. In the future, more materials would provide a better insight to the accuracy of the EI term as a measure of stiffness. Further testing with different lengths of materials and would further support this. Due to the existence of some outliers on each of the graphs, additional testing with these parameters could also provide useful information. More than twelve tests per set of parameters may be helpful for future experiments as well. Variations on the ratio of the intruder thickness to the grain size would help extrapolate the data into different media.

With the data from future experiments, this data can be analyzed to determine the best way to stabilize soil with flexible intruders. The initial trends from these experiments indicate that less stiff intruders both provide more energy efficiency in granular material and longer force chains. An ideal material for large-scale soil stabilization also has yet to be determined. Variations in the maximum force applied will also affect the summed forces in the system, the maximum intruder depth, and the energy applied to the system, and will need to be explored further. With additional laboratory and field testing, the optimum parameters for soil stabilization can be determined.

6. CONCLUSIONS

While flexible intruders have a comparable affect to pinto bean roots on their surrounding environment, a flexible intruder inserted up to a force of 1 N exerts a mean force of .028 N on its surrounding environment, approximately three times the force a pinto bean root exerts. Because of this, a flexible intruder may be more effective at soil stabilization in highly erosive conditions than certain types of root. Further data on the forces exerted by other types of root may help with additional research of the flexible intruder.

In addition, several trends with respect to the stiffness of the flexible intruders, in this case in terms of EI, have been demonstrated. Increasing stiffness corresponds to an increased force on the particles that are stressed. However, increasing stiffness also corresponds to fewer particles overall being stressed, and thus shorter force chains. Additionally, less stiff flexible intruders, especially those near buckling, provide a much greater efficiency between the energy applied to the system and the energy present in the system during the peak force applied.

Future experiments will be needed to further develop the requirements for appropriate soil stabilizing flexible intruders. The proximity of buckling and the likelihood of buckling will both need to be taken into account. The material used and number of experiments run should also be further explored. Parameters such as maximum force, system size, intruder length, and grain size should also be considered in order to extrapolate these results to a real-world soil setting.

REFERENCES

[1] Genet, Marie, et al. *Eco-and Ground Bio-Engineering: The Use of Vegetation to Improve Slope Stability*. Springer. 2007

[2] D.M. Wendell, et al. *Experimental Investigation of Plant Root Growth through Granular Substances*. Springer, 0014-4851.

APPENDIX A

The determination of the forces between particles was done in MATLAB, using a multistep process. The MATLAB code first cropped and rotated the images. The center of each image was found by taking the green layer of the rgb image and changing it to a black and white image. In order to make certain that the system was a solid color in the binary image, the imerode and imdilate functions were used, and the center of the resulting mass found. MATLAB code then changed the red layer of the rgb image into a black and white image, and, starting at that center, proceeded in all directions until it reached the red border around the system. The points at which the red border started on the bottom were recorded. These points were then fitted to a line, the slope of which was used to determine the angle the picture was tilted. The image was then rotated using MATLAB's imrotate function. The modal distance between each of the red enamel borders and the edges of the picture, within a tolerance of 5 pixels, was recorded. The image was then cropped by the appropriate distance on each side. As the ratio of the width of the cropped image to the particle radius was known, the particle radius was also calculated.

From the cropped images, the location of every particle center was determined. The green layer of the rgb image was once again selected. In order to determine the appropriate function, the green image was processed with a variety of grayscale to black and white thresholds, starting at 0.1 and increasing in increments of 0.02. The number of particle centers located each time was recorded. As many particles (more than 15) were used, and these particles had a known radius, the threshold value that found the maximum number of particles was determined to be the most accurate threshold. In order to find the centers for an image with a given threshold, the image was changed to black and white with that threshold. The imerode function was then used to separate the particles, and the imdilate function was used to return the particle images to a circular shape. The regionprops function was again used to determine the locations of the centers of the particles. Particles were determined to be in contact if their centers were closer together than 2.2 times the particle radius.

In order to calculate the forces between particles, the color gradient everywhere in the photograph was determined. The color gradient at each pixel was calculated for each of the rgb color matrices to give an rgb image of the intensity. This rgb image was then converted to a grayscale image using Formula 1 for the intensity at each point. In this equation, j_r, j_g, and j_b were the intensities of each pixel in the red, green, and blue layers, respectively, and j was the resulting overall intensity. This formula was used to minimize noise, as noise was equivalent across all three colors. As this formula did not remove the color gradient from the edges of the particles, the color gradient image was then modified to only contain the color gradients within (radius-10) pixels of any particle center.

$$j = \sqrt{(j_r - j_g)^2 + (j_g - j_b)^2 + (j_b - j_r)^2} \qquad \text{Formula 1}$$

Because of where the photoelastic particles generate high color gradients, the relevant gradient was determined using the average pixel color gradient close to points where particles were in contact. For each pair of particles in contact, two circular areas were used to compute the average color gradient. These areas were centered 1/3 of the way from one particle center to the other center, and had a radius of .364 times the radius of a particle. If the two average intensities had a large discrepancy, the value for that contact was set to the lesser value. Otherwise, the value for the given contact was set to the average of the two values.